

## CHAPTER 242

### Measurements of Wave Generated Bedforms

Christopher D. Jetté<sup>1</sup> and Daniel M. Hanes<sup>2</sup>

#### Abstract

A 5 MHz multiple transducer array was used to measure wave generated bedforms near Duck, NC. The transducer array consists of 37 transducers with a center to center spacing of 1.2 centimeters. Seabed measurements were made with approximately 1 millimeter vertical and 2 centimeter horizontal resolution. Measured ripple dimensions are compared to three popular ripple prediction models. It is shown that errors of over 100 percent were found between measured and predicted ripple heights and lengths for all ripple models compared. Errors in predicting ripple steepness ranged from 37 to 55 percent.

#### Description Of Experiment

Field measurements of bedforms were made during an experiment at the Army Corps of Engineers Field Research Facility in Duck, NC during August 23-25, 1995. The instruments were deployed using a Sensor Insertion System (SIS) on the research pier. The SIS was positioned at multiple locations along the cross-shore profile during the experiment.

Bedform measurements were made using a multiple transducer array (MTA) developed at the University of Florida. The MTA consists of 37 ultra-sonic transducers operating at a frequency of 5 MHz. The center-to-center spacing of the transducers is 12 mm. Such configuration allows for O(1 mm) vertical resolution and O(2 cm) horizontal resolution. The MTA can scan a profile in approximately 4 seconds. The distance to the seabed is calculated from the elapsed time between the pulsing of the transducer and the time at which the return exceeds a software selectable threshold.

- 
- 1) Research Assistant, Department of Coastal and Oceanographic Engineering, University of Florida, PO Box 116590, Gainesville, FL 32611, USA.
  - 2) Associate Professor, Department of Coastal and Oceanographic Engineering, University of Florida, PO Box 116590, Gainesville, FL 32611, USA.

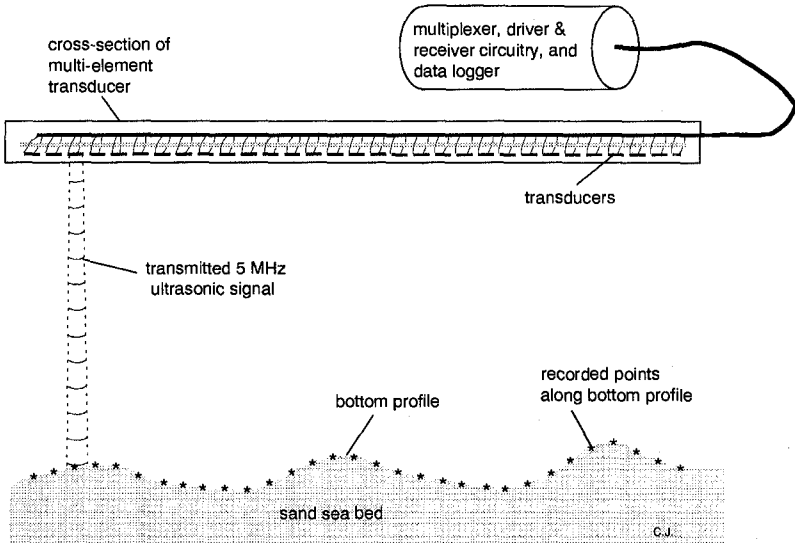


Figure 1. Schematic of the MTA

In addition to the MTA, an under-water video camera was deployed in order to document bedform orientation. Electro-magnetic current meters and pressure transducers were deployed to measure the wave and current conditions. Measurements of the vertical distribution of suspended sediment by acoustical backscatter methods were also made.

The data was collected in 13 minute bursts. Each burst contained 131 profiles taken with the MTA. Current, pressure, and concentration profile data were collected at 4 Hz.

### Conditions During Experiment

Exploiting the mobility of the SIS, measurements were made under a variety of wave and sediment conditions. During the experiment, an off-shore bar was present at approximately 210 meters from the high water line. Measurements were made at 8 separate cross-shore locations in the regions offshore of the bar, on the bar, in the trough, and on the nearshore beach-face. Depths where measurements were made ranged from 1.6 to 6.8 meters. The vertical lines in figure 2 indicate cross-shore locations where measurements were obtained.

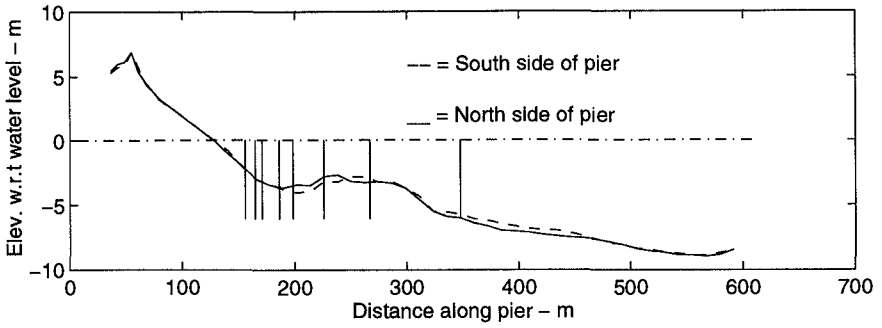


Figure 2. Cross-shore profiles from North and South sides of pier during experiment.

The sediment characteristics varied greatly over the cross-shore profile.  $D_{50}$  values of the mostly quartz sediment ranged from 0.19 to 1.67 mm. The range of  $D_{50}$  values versus run number are plotted in Figure (3) along with  $H_{m0}$  (a), peak wave period (b), and water depth (c).

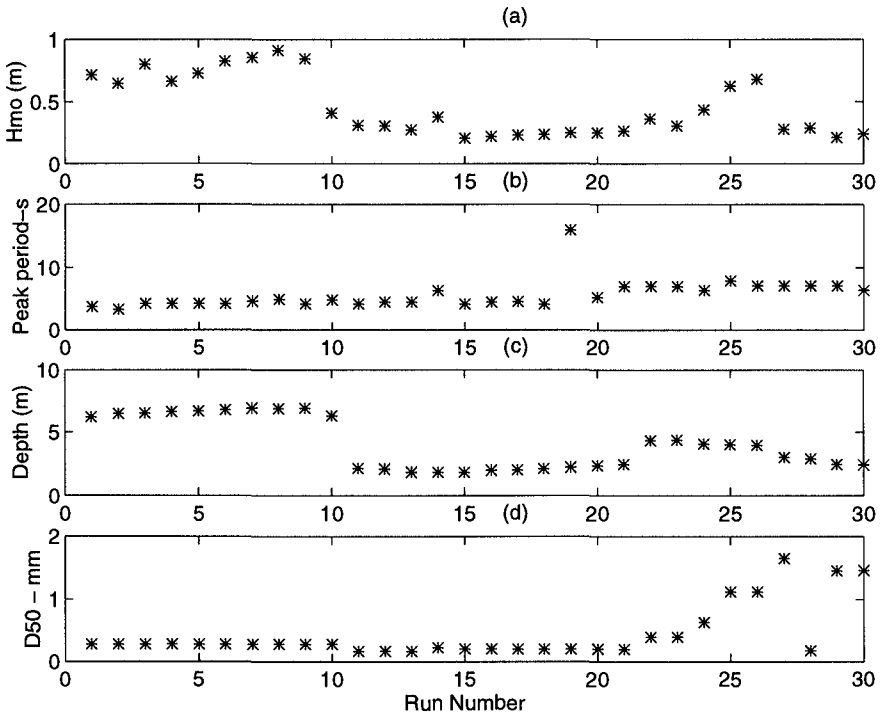


Figure 3.  $H_{m0}$  (a), peak wave period (b), water depth (c), and  $D_{50}$  (d) vs. Run number for SIS experiment

Most of the wave data taken over the three day period contained at least two, if not three frequency peaks in the surface elevation spectrum. For many of the runs there was a low frequency component (12-15 sec. period) generated from hurricane Felix, which was several hundred miles off-shore, as well as a moderate frequency component (6-8 sec. period), and generally in the afternoon, a higher frequency (4-5 sec. period) locally generated component.  $H_{m0}$  wave heights varied from 0.2 to 0.9 meters. During most of the experiment the predominate wave direction at the experiment site was directly on-shore.

For most of the runs measurements were made offshore of the breakpoint, however during runs 11 through 21 some waves were noted to break in the vicinity of the instruments. It is also noted that, after transforming the pressure spectrums into surface elevation spectrums, in the majority of cases the higher frequency component became the peak frequency. Consequently, the wave period used in model prediction was the lowest period component in the wave profile.

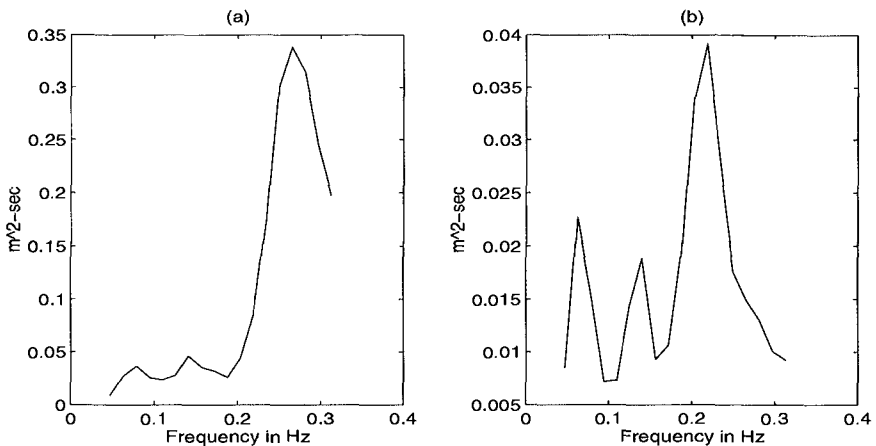


Figure 4. Representative corrected surface elevation spectrums from SIS experiment for runs 1 (a) and 13 (b) with  $H_{m0}$  wave heights of 0.72 and 0.28 meters respectively

### Measurements

Bedforms were present throughout the experiment, however their geometries varied greatly over the beach profile. Measured bedform heights ranged from 7 to 50 mm, and bedform lengths ranged from 80 to 1000 mm. Active ripple conditions were observed during all times of data collection. For most of the files under-water video was available to document near-bed sediment motion and ripple orientation. Significant ripple migration was not observed during any of the 13 minute runs.

Bedform profiles were collected at a rate of ten profiles per minute. For the measurements presented herein, a single representative profile was found for each minute of data (10 scans). An example of the thirteen representative profiles for an entire run is shown in figure 5 (a-c). In these figures, each profile has been offset by -3 mm from the previous profile for comparative display. The top profile represents the first minute of data and contains circles at each of the 37 measured data points.

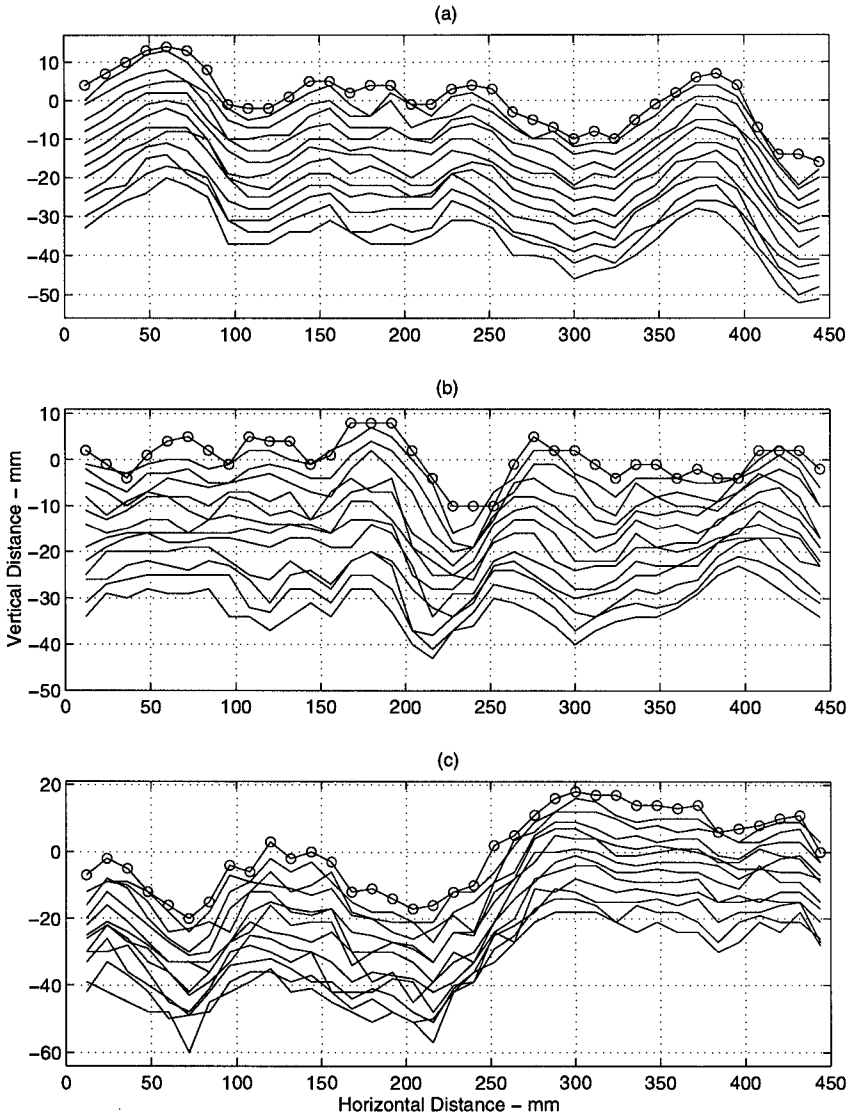


Figure 5. Representative profiles for each minute of a 13 minute run from runs 1(a), 13(b), and 26(c). Data from first minute of run is plotted with circles.

In order to compare these data to models, the bedforms need to be characterized in terms of a wavelength and height. In previous work this has typically been accomplished by visual inspection. We therefore chose a threshold method to determine ripple height and length dimensions for each representative ripple profile. This method first found the peaks and troughs along a profile. Then, if the distance between adjacent peaks and troughs met a certain threshold criterion, they were recorded. From these peaks and troughs average ripple heights and lengths were found. The threshold was chosen conservatively, that is, to maximize ripple heights and lengths. Figure (6) is an example of a representative profile with the threshold ripple crests and troughs marked.

Table 1. Measured hydrodynamic parameters and ripple dimensions for field experiment.

run	loc. (m)	depth (m)	Hmo (m)	Tp (s)	D50 (mm)	ltm(1) (mm)	ltm(4) (mm)	ltm(8) (mm)	ltm(13) (mm)	h <sub>m</sub> (1) (mm)	h <sub>m</sub> (4) (mm)	h <sub>m</sub> (8) (mm)	h <sub>m</sub> (13) (mm)
1	347	6.10	0.71	3.76	0.28	103	81	103	107	13	11	13	14
2	347	6.33	0.65	3.76	0.28	103	103	82	105	13	13	12	13
3	347	6.42	0.80	4.27	0.28	100	106	101	106	14	14	12	16
4	347	6.53	0.66	4.27	0.28	108	107	101	154	13	13	14	19
5	347	6.58	0.73	4.27	0.28	107	103	101	105	14	14	15	14
6	347	6.69	0.83	4.27	0.28	152	150	147	149	18	19	16	17
7	347	6.78	0.85	4.57	0.28	103	146	144	105	12	16	16	12
8	347	6.79	0.92	4.92	0.28	98	136	95	104	12	14	10	12
9	347	6.82	0.85	4.27	0.28	158	164	154	152	18	17	17	17
10	347	6.16	0.41	4.92	0.28	102	102	101	102	14	14	15	14
11	267	1.94	0.31	4.27	0.18	112	112	113	115	10	10	9	11
12	267	1.90	0.31	4.57	0.18	117	86	89	113	10	11	10	12
13	267	1.62	0.27	4.57	0.18	84	110	110	105	10	11	14	13
14	267	1.65	0.38	6.40	0.24	1000	1000	1000	1000	50	50	50	50
15	226	1.63	0.21	4.27	0.21	77	101	97	94	8	9	11	10
16	226	1.76	0.22	4.57	0.21	102	99	106	124	13	13	14	16
17	226	1.82	0.23	4.57	0.21	94	90	88	113	11	12	11	11
18	226	1.91	0.24	4.27	0.21	107	139	97	113	8	11	10	12
19	226	1.99	0.26	16.00	0.21	70	86	84	82	9	10	8	10
20	226	2.14	0.25	5.33	0.21	83	83	83	83	7	7	7	7
21	226	2.25	0.27	7.11	0.21	101	101	101	101	11	11	11	11
22	198	4.19	0.37	7.11	0.40	275	275	275	275	40	40	40	40
23	198	4.21	0.31	7.11	0.40	275	275	275	275	40	40	40	40
24	186	3.90	0.44	6.40	0.64	240	232	224	240	26	28	28	26
25	186	3.86	0.63	8.00	1.12	136	134	138	131	23	20	22	20
26	186	3.80	0.69	7.11	1.12	146	147	154	154	23	25	23	23
27	171	2.80	0.28	7.11	1.66	144	136	127	139	15	15	16	15
28	165	2.72	0.29	7.11	0.18	500	500	500	500	45	45	45	45
29	155	2.25	0.22	7.11	1.47	197	108	103	120	27	17	17	17
30	155	2.20	0.24	6.40	1.47	117	128	106	125	18	17	16	17

For model comparisons, each run of data was summarized into four profiles. These profiles were from minutes 1, 4, 8, and 13 of each 13 minute run. The reasons for this were to minimize the amount of clutter in model comparisons, while at the

same time retain the range of ripple geometries present during each run. Measured ripple length (ltm) and height (htm) along with summaries of hydrodynamic and sediment conditions are presented in table 1 for each run.

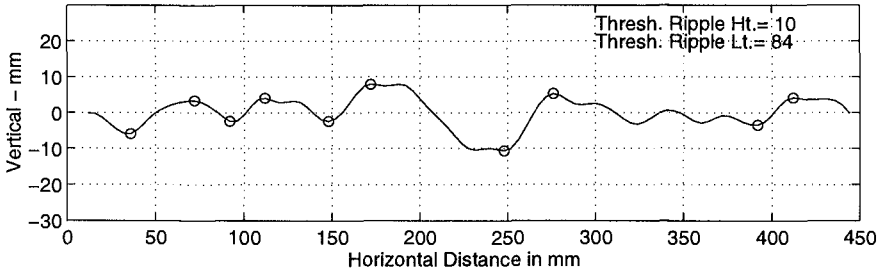


Figure 6. Representative ripple profile with threshold method results for first minute of data from run number 13.

Model Comparisons

Measured bedform dimensions were compared to three predictive models; Nielsen (1981), Wiberg and Harris (1994), and Grant and Madsen (1981). For each run measured values of water depth, Hmo wave height, peak period, and sediment properties were entered into the predictive models. Measured bedform dimensions were plotted with the model curves, if possible, in order to better illustrate the relationships between measured values and predicted values.

Nielsen (1981) derived different predictive models for regular (laboratory) and irregular (field) conditions. Comparisons included herein refer to the irregular or field ripple models. The Nielsen (1981) bedform model characterizes flow conditions using sediment mobility number ( $\Psi$ ), grain roughness Shield’s parameter ( $\theta_{2.5}$ ), and the wave friction factor “ $f_{2.5}$ ” given by Swart (1974). These parameters are defined as follows

$$\theta_{2.5} = 0.5 f_{2.5} \psi \tag{equation 1}$$

$$f_{2.5} = \exp \left[ 5.213 \left( \frac{2.5 D_{50}}{A} \right)^{0.194} - 5.977 \right] \tag{equation 2}$$

$$\psi = \frac{(a \omega)^2}{(s - 1) g D} \tag{equation 3}$$

where “D” is the mean grain diameter, “a” is the near-bed wave semi-excursion, “s” is the sediment specific gravity, “g” is the acceleration of gravity, and  $\omega$  is the

angular frequency of the waves. The Nielsen (1981) irregular wave model for non-dimensional ripple steepness, height, and length are respectively

$$\eta/\lambda = 0.342 - 0.34(\theta_{2.5})^{0.25} \quad \text{equation 4}$$

$$\eta/a = 21\Psi^{-1.85} \quad \text{for } \Psi > 10 \quad \text{equation 5}$$

$$\eta/a = 0.275 - 0.022\Psi^{0.5} \quad \text{for } \Psi < 10 \quad \text{equation 6}$$

$$\lambda/a = \exp\left[\frac{693 - 0.37\ln^8\Psi}{1000 + 0.75\ln^7\Psi}\right] \quad \text{equation 7}$$

where  $\eta$  and  $\lambda$  represent ripple height and length respectively.

Relationships between measured ripple dimensions and the Nielsen (1981) model curves are illustrated in figure (8). As can be seen in figure 8(a), for all but 5 out of the 30 runs the Nielsen (1981) irregular wave ripple model over-predicted ripple height. The largest amount of over-prediction was found to occur at low values of sediment mobility number ( $\Psi < 20$ ). The Nielsen (1981) ripple length model agreed best with measured dimensions for higher values of mobility number ( $\Psi > 12$ ), however for lower values of mobility number ( $\Psi < 12$ ), the model over-predicted ripple length for all runs. Measurements of ripple steepness had better agreement with the Nielsen (1981) model curves than did ripple height or ripple length. Best agreement was found at higher values of the grain roughness Shield's parameter ( $\theta_{2.5} > 0.08$ ). For lower values of the Shield's parameter the Nielsen (1981) model over-predicted ripple steepness.

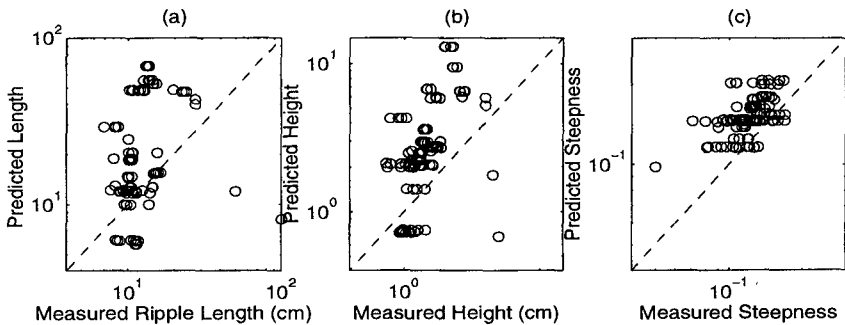


Figure 7. Nielsen (1981) irregular wave ripple comparison with measurements

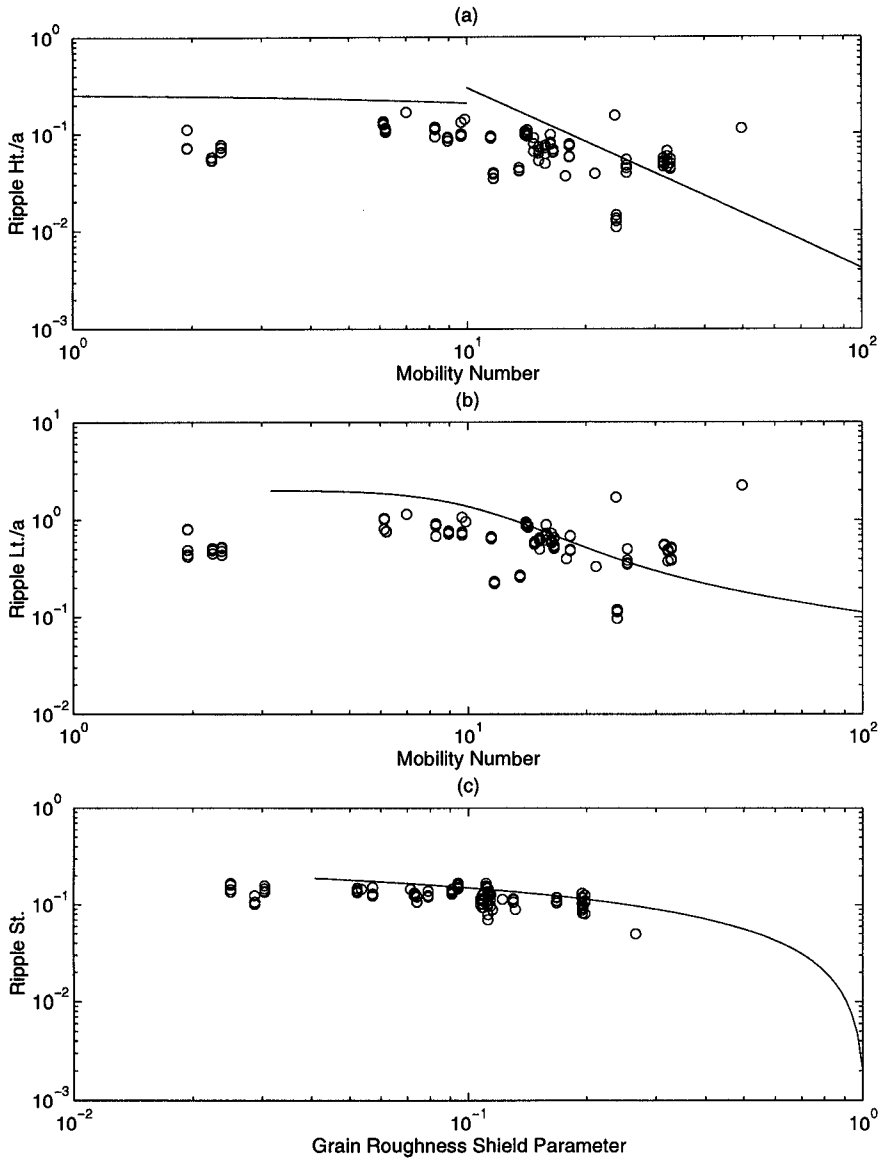


Figure 8. Comparison of measured field ripple dimensions and Nielsen (1981) model curves for height (a), length (b), and steepness (c).

Wiberg and Harris (1994) reexamined existing ripple data from oscillatory flows in both flume and field studies to construct a model to predict ripple geometry for all types of oscillatory flow environments. Wiberg and Harris (1994) classified

bedforms according to the ratio of the wave boundary layer thickness and ripple height ( $d_o/\eta$ ). From this ratio, the ripples were classified as orbital, anorbital, or suborbital by the following criteria

Table 2. Wiberg and Harris (1994) ripple classification

flow conditions	ripple classification
$d_o/\eta_{ano} < 20$	orbital ripples
$20 < d_o/\eta_{ano} < 100$	suborbital ripples
$d_o/\eta_{ano} > 100$	anorbital ripples

The Wiberg and Harris (1994) equations for ripple length and steepness for orbital ripples are:

$$\lambda_{orb} = 0.62d_o \quad \text{equation 8}$$

$$(\eta/\lambda)_{orb} = 0.17 \quad \text{equation 9}$$

for anorbital ripples

$$\lambda_{ano} = 535 D \quad \text{equation 10}$$

$$\frac{\eta}{\lambda} = \exp \left[ -0.095 \left( \ln \frac{d_o}{\eta} \right)^2 + 0.442 \ln \frac{d_o}{\eta} - 2.28 \right] \quad \text{for } d_o/\eta > 10 \quad \text{equation 11}$$

and for suborbital ripples

$$\lambda_{sub} = \exp \left[ \left[ \frac{\ln \left( \frac{d_o}{\eta_{ano}} \right) - \ln 100}{\ln 20 - \ln 100} \right] \left( \ln \lambda_{orb} - \ln \lambda_{ano} \right) + \ln \lambda_{ano} \right] \quad \text{equation 12}$$

where “ $d_o$ ” is the near bottom orbital diameter, and “ $D$ ” is the mean sediment size.

In figure (9), measured non-dimensional ripple dimensions are plotted versus the parameters used in the Wiberg and Harris (1994) ripple model. Where possible, the model curves were included. It is noted that in figure (9d) the x-axis is near bottom orbital diameter divided by measured ripple height. For these plots, the dashed and solid curves refer to the orbital and anorbital ripple models respectively. The data in figure (9) is also plotted according to the Wiberg and Harris (1994) ripple classification scheme. Each data point is plotted as an “o”, “+”, or “\*” indicating ripple types of orbital, suborbital, or anorbital ripples, respectively. The Wiberg and Harris (1994) model also over-predicted ripple length and height for most of the runs. It is also interesting to note that only 2 of the 30 runs were classified as anorbital ripples.

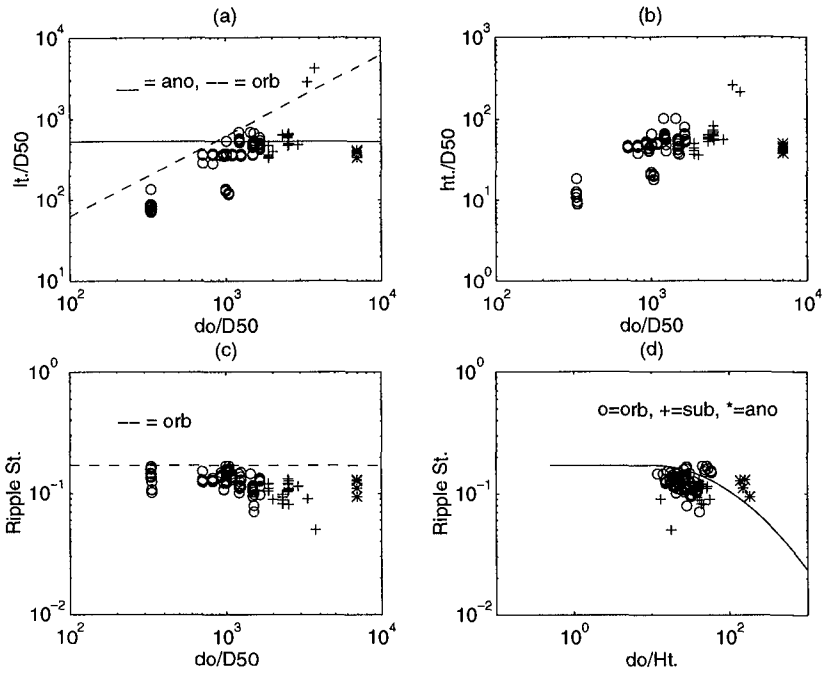


Figure 9. Wiberg and Harris (1994) ripple models with measured values.

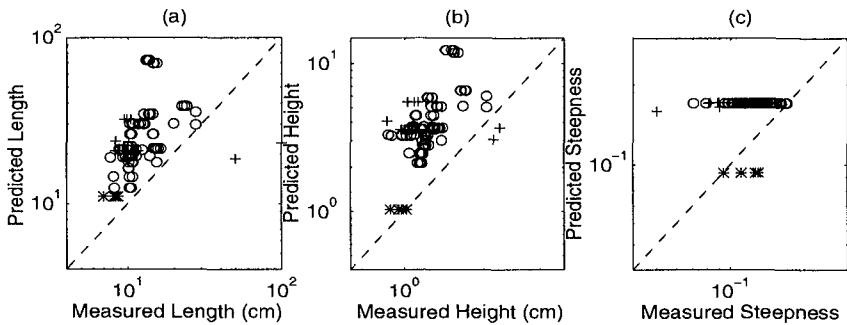


Figure 10. Wiberg and Harris (1994) model ripple comparison with measurements

The Grant and Madsen (1982) ripple model uses the ratio of the maximum value of the skin friction (shear stress) under the wave ( $\tau_{*sf}$ ) to the critical value of shear stress for the initiation of sediment motion ( $\tau_{*cr}$ ). Also a dimensionless sediment parameter ( $S_*$ ) is used. This ripple model was based primarily on the Carstens et al. (1969) laboratory oscillatory ripple study.

Two separate regions of transport stages were used in the Grant and Madsen (1982) model. The first stage, when the flow conditions are less than the breakoff point defined by equation (18), is known as the equilibrium stage. Within the equilibrium range, ripple steepness is a maximum and the ripple length is said to scale with the near-bottom excursion amplitude. When flow conditions exceed the breakoff point, conditions are said to be in the breakoff region; the ripple length is said to no longer be in equilibrium and a decorrelation between ripple length and near-bottom excursion amplitude occurs (Grant and Madsen (1982)). As the flow intensity increases within the breakoff region, ripple steepness continues to decrease to a point where ripples are no longer present.

The Grant and Madsen (1982) ripple prediction model is as follows:  
when the transport stage is less than the breakoff point

$$\eta/\lambda = 0.16 \left( \tau_{*sf} / (\tau_*)_{cr} \right)^{-0.04} \quad \text{equation 13}$$

$$\eta / a_o = 0.22 \left( \tau_{*sf} / (\tau_*)_{cr} \right)^{-0.16} \quad \text{equation 14}$$

and at higher transport stages, above the breakoff range

$$\eta/\lambda = 0.28 S_*^{0.6} \left( \tau_{*sf} / (\tau_*)_{cr} \right)^{-1.0} \quad \text{equation 15}$$

$$\eta / a_o = 0.48 S_*^{0.8} \left( \tau_{*sf} / (\tau_*)_{cr} \right)^{-1.5} \quad \text{equation 16}$$

where

$$S_* = (d / 4\nu) [(S - 1)gD]^{0.5} \quad \text{equation 17}$$

and the breakoff point is defined as

$$\left[ \tau_{*sf} / (\tau_*)_{cr} \right]_B = 1.8 S_*^{0.6} \quad \text{equation 18.}$$

where 'v' is the kinematic viscosity of water, 'D' is the grain diameter, 'S' is the specific gravity of the sediment, and 'g' is the acceleration of gravity.

A comparison of Grant and Madsen (1982) predicted ripple heights and lengths versus measured values is shown in figure 11. It can be seen that the Grant and Madsen (1982) model overpredicted ripple length and height for almost every run.

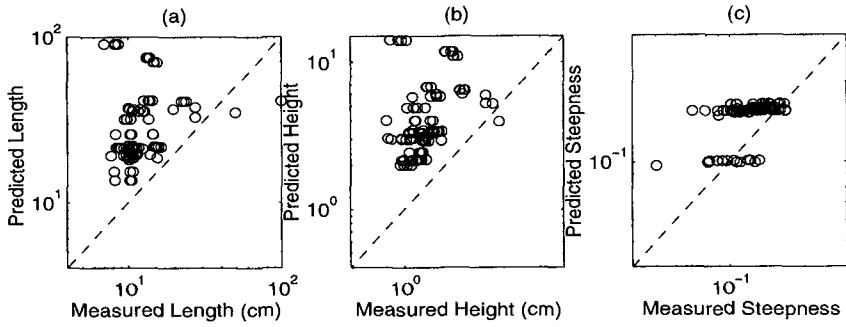


Figure 11. Grant and Madsen (1982) model ripple comparison with measurements

In order to evaluate the performance of the predictive models, the relative error was computed between measured and predicted values. The relative error is defined as:

$$\Delta = \exp \left\{ \left[ \frac{1}{n} \sum_1^n (\ln(y) - \ln(\hat{y}))^2 \right]^{1/2} \right\} \quad \text{equation 19}$$

where  $y$  is the measured value and  $\hat{y}$  is the predicted value. This quantity is a multiplicative factor that indicates the possible variation about the predicted value (Wikramanayake, 1993). For example if  $\Delta$  equals 1.34, the average error is equal to 34 percent.

Table 3 contains values of the relative error for each of the different predictive models. It can be seen that the predictive models performed much better at predicting ripple steepness than ripple height or length independently. The Nielsen (1981) and Grant and Madsen (1982) ripple steepness models performed the best at predicting ripple steepness with an average error of 37 percent, the Wiberg and Harris (1994) model had an average error of 55 percent. The Nielsen (1981) model predicted ripple height the best, however the average error was found to be 153 percent. The Wiberg and Harris (1994) and Grant and Madsen (1982) models had even greater error. Ripple length comparisons showed the Wiberg and Harris (1994) model having the least error with an average error of 125 percent. The Nielsen (1981) and Grant and Madsen (1982) ripple length models had slightly higher relative errors with 150 and 154 percent respectively.

TABLE 3. Relative Error for model predictions and measured values.

	Ripple Length	Ripple Height	Ripple Steepness
Nielsen (1981) Field	2.50	2.53	1.37
Wiberg & Harris (1994)	2.25	2.84	1.55
Grant and Madsen (1982)	2.54	3.03	1.37

## Conclusions

The multiple transducer array (MTA) has proven the ability to measure bedforms in the field environment with  $O(1 \text{ mm})$  vertical and  $O(2 \text{ cm})$  horizontal resolution. Comparisons of oscillatory field ripple data collected with the MTA and the most popular predictive models show errors of over 100 percent for all models in predicting ripple heights and lengths. Average errors of 37 to 55 percent were found in predicting ripple steepness. Such errors could be due to errors in the previously collected data sets used to construct these models, or to the current understanding of the mechanics of ripple formation and geometric equilibrium with the flow field. More investigation is necessary in this field in order to improve bedform prediction models.

## Acknowledgments

The authors wish to acknowledge the financial support of the U.S. Office of Naval Research, Coastal Sciences Program, the field assistance provided by the Field Research Facility, U.S. Army Corps of Engineers, and the help of Chuck Broward, Eric Thosteson, Mike Krecic, and Carl Miller.

## References

- Bagnold, R. A., Motion of waves in shallow water: Interaction between waves and sand bottoms, Proc. R. Soc. London Ser. A, 187, 1-15, 1946.
- Carstens, M. R., R. M. Neilson, and H. D. Altinbilek, Bed forms generated in the laboratory under oscillatory flow: Analytical and experimental study, Tech. Memo. 28, U.S. Army Corps of Eng., Coastal Eng. Res. Center, June 1969.
- Dingler, J. R., and Inman D. L., Wave-formed ripples in near-shore sands, Proc. Fifteenth Conf. Coastal Engng., Amer. Soc. Civil Eng., 1976.
- Grant, W. D., and O. S. Madsen, Movable bed roughness in unsteady oscillatory flow, J. Geophys. Res., 87, 469-481, 1982.
- Nielsen, P., Dynamics and geometry of wave-generated ripples, J. Geophys. Res., 86, 6467-6472, 1981.
- Nielsen, P., Field measurements of the time-averaged suspended sediment concentration under waves. Coastal Engng., 8, 51-72, 1984.
- Sleath, J. F. A., Sea bed mechanics, Wiley Interscience, New York, 1984.
- Swart, D. H., Offshore sediment transport and equilibrium beach profiles. Delft Hydr. Lab. Publ. No. 131, 1974.
- Vincent, C. E., and P. D. Osbourne, Bedform dimensions and migration rates under shoaling and breaking waves, Unpublished manuscript (1992).
- Wiberg, P.L., and C. K. Harris, Ripple geometry in wave dominated environments, J. Geophys. Res., 99, 775-789, 1994.
- Wikramanayake, P. N., Velocity profiles and suspended sediment transport in wave-current flows. Ph.D. Thesis. Dept. of Civil Eng., MIT, Cambridge, Mass., 1993.